Author/s:
Peterson, TJ;Western, AW

Title:
Multiple hydrological attractors under stochastic daily forcing: 1. Can multiple attractors exist?

Date:
2014-04-01

Citation:
Peterson, T. J. & Western, A. W. (2014). Multiple hydrological attractors under stochastic daily forcing: 1. Can multiple attractors exist?. WATER RESOURCES RESEARCH, 50 (4), pp.2993-3009. https://doi.org/10.1002/2012WR013003.

Persistent Link:
https://hdl.handle.net/11343/297403

AGU PUBLICATIONS

Water Resources Research

RESEARCH ARTICLE
10.1002/2012WR013003

Companion to *Peterson et al.* [2014], doi:10.1002/2012WR013004.

Key Points:
- Multiple hydrological attractors can exist under daily climate forcing
- Daily forcing reduces the likelihood of multiple attractors
- Monthly, or annual, forcing produces inaccurate estimates of attractors

Supporting Information:
- Readme file
- Matlab model and input data

Correspondence to:
T. J. Peterson,
timjp@unimelb.edu.au

Citation:
Peterson, T. J., and A. W. Western (2014), Multiple hydrological attractors under stochastic daily forcing: 1. Can multiple attractors exist?, *Water Resour. Res.*, *50*, 2993–3009, doi:10.1002/2012WR013003.

Received 25 SEP 2012
Accepted 4 MAR 2014
Accepted article online 10 MAR 2014
Published online 8 APR 2014

Multiple hydrological attractors under stochastic daily forcing: 1. Can multiple attractors exist?

T. J. Peterson[1] and A. W. Western[1]

[1]Department of Infrastructure Engineering, University of Melbourne, Parkville, Victoria, Australia

Abstract Including positive feedbacks in hydrological models has recently been shown to result in complex behavior with multiple steady states. When a large disturbance, say a major drought, is simulated within such models the hydrology changes. Once the disturbance ends the hydrology does not return to that prior to the disturbance, but rather, persists within an alternate state. These multiple steady states (henceforth *attractors*) exist for a single model parameterization and cause the system to have a finite resilience to such transient disturbances. A limitation of past hydrological resilience studies is that multiple attractors have been identified using mean annual or mean monthly forcing. Considering that most hydrological fluxes are subject to significant forcing stochasticity and do not operate at such large timescales, it remains an open question whether multiple hydrological attractors can exist when a catchment is subject to stochastic daily forcing. This question is the focus of this paper and it needs to be addressed prior to searching for multiple hydrological attractors in the field. To investigate this, a previously developed semi-distributed hillslope ecohydrological model was adopted which exhibited multiple steady states under average monthly climate forcing. In this paper, the ecohydrological model was used to explore if feedbacks between the vegetation and a saline water table result in two attractors existing under daily stochastic forcing. The attractors and the threshold between them (henceforth *repellor*) were quantified using a new limit cycle continuation technique that upscaled climate forcing from daily to monthly (model and limit cycle code is freely available). The method was used to determine the values of saturated lateral hydraulic conductivity at which multiple attractors exist. These estimates were then assessed against time-integration estimates, which they agreed with. Overall, multiple attractors were found to exist under stochastic daily forcing. However, changing the climate forcing from monthly to daily did significantly reduce the parameter range over which two attractors existed. This suggests fewer catchments may have multiple attractors than previously considered.

1. Introduction

Recently, a number of studies have investigated multiple ecohydrological steady states. The concepts emerge from the field of ecosystem resilience and consider ecosystems in which a temporary disturbance causes a change in the system that persists long after the disturbance ends; that is, the system persists within an alternative steady state. Figure 1 illustrates a system with two steady states. The system state oscillates around one steady state for a period of time in response to forcing disturbances. When a sufficiently large and long disturbance occurs it crosses the threshold between the steady states and moves to a new region in the state space and oscillates around a second steady state, even though the system forcing has returned to its original levels. This can occur in systems where there is a positive feedback within the system dynamics. These steady states are often referred to as attractors and the system tends toward these attractors under average forcing conditions. In this context, the concept of resilience refers to the size of a disturbance required to bring about a change of state from one steady state or attractor to another. Few hydrological models include a positive feedback and those without a positive feedback exhibit infinite resilience. That is, they will return back to a similar state once an infinitely large disturbance is removed.

Ecological modeling of multiple attractors and resilience began with *Holling* [1973] and *May* [1977]. In a hydrological context, identifying the attractors can inform how a catchment may respond to and recover from disturbances such as droughts, floods, or groundwater pumping. For a model of such a catchment, two steady states (henceforth referred to as *attractors*) would exist if, for the same parameter set and climate forcing, two different time series of streamflow, groundwater level or soil moisture could be derived.

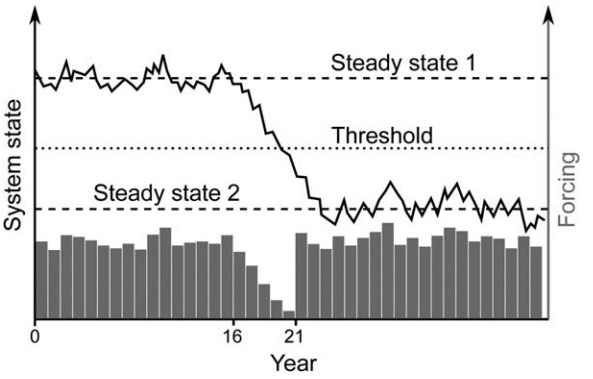

Figure 1. Illustration of a system with two steady states and the switching between the steady states as a result of stochastic forcing. It shows the two steady states (i.e., attractors) that exist under average forcing and the threshold between the steady states (i.e., repellor). As a result of stochastic forcing, the system state fluctuates. From years 16 to 20, a large disturbance occurs (e.g., a drought) and the system state declines to below the threshold. In year 21, the large disturbance ends but the system state converges to the lower steady state and then persists near to it for the remaining years. For this illustration, both steady states did emerge because stochastic forcing was sufficient to cause switching between both steady states. Note that this figure illustrates the interaction between multiple steady states and stochastic forcing according to standard resilience concepts [*Walker et al*., 2004; *Guttal and Jayaprakash*, 2007; *Beisner et al*., 2003]. These concepts are challenged within the companion paper (Peterson et al., –submitted manuscript, 2013).

Between the state space location of the attractors is a threshold (henceforth *repellor*) and according to standard resilience concepts [*Walker et al*., 2004; *Guttal and Jayaprakash*, 2007; *Beisner et al*., 2003], the system switches attractors by disturbances perturbing it past the repellor. Quantitative investigation of such dynamics have been undertaken in the context of vegetation-soil moisture interactions [*D'Odorico et al*., 2005; *Guttal and Jayaprakash*, 2007; *D'Odorico et al*., 2008]; unconfined aquifer-vegetation interactions [*Peterson*, 2009; *Peterson et al*., 2009; *Anderies*, 2005; *Ridolfi et al*., 2006; *Runyan and D'Odorico*, 2010]; wetlands [*D'Odorico et al*., 2011; *Heffernan*, 2008]; and peatlands [*Rennermalm et al*., 2010]. However, a weakness of many of these studies is that stochastic climate forcing was ignored in the identification of the multiple attractors. Considering that stochastic forcing strongly influences the behavior of nonlinear fluxes, such as infiltration, runoff, and recharge, its complete omission or its inclusion at an inappropriate time scale potentially invalidates the findings of multiple hydrological attractors. If theories of hydrological systems having multiple attractors are to advance beyond modeling studies to the identification of multiple attractors in the field, it is important to first determine if multiple attractors can exist when realistic (stochastic) forcing is input to sufficiently realistic hydrological models. This question is investigated in this paper using a hypothetical coupled vadose zone-hillslope Boussinesq model.

Ideally, the investigation would have been undertaken for a real catchment using only observation data or a calibrated model. However, selecting such a study catchment would be challenging considering that it is unknown if, and for what type of catchment, multiple attractors may exist. Furthermore, to provide evidence of multiple hydrological attractors occurring in the field, the study catchment would have had to experience a climate sequence causing a switch of attractors and a means would need to exist to identify such a switch from, often very noisy, hydrological data. Considering that it is also unknown what hydrological signatures would be indicative of a switch, it would have been premature to undertake a field study. By first undertaking a hypothetical modeling study, the complex interactions between stochastic climate, hydrological properties, catchment geometry and the positive feedback between vegetation and the water table could be explored to identify if, and when, multiple attractors can exist and, importantly, the hydrological signatures indicative of a change of attractors. If multiple attractors are found to exist and the hydrological system can switch between those attractors, then field studies would be appropriate and the findings from the hypothetical modeling could be used to assist in designing the field analysis.

The existence of multiple attractors, however, provides no insight into if or how often the catchment might switch between the attractors. For example, if the climatic disturbances are *insufficient* then, for a given parameter set, the catchment may converge to and persist within, say, a deep water table attractor; making a second shallow water table attractor practically superfluous. Alternatively, climatic disturbances may be *sufficient* to cause repeated switching between the attractors; hence causing an amplified hydrological response to climate variability. Such repeated switching has been shown to occur using a very simple 1-D groundwater model, but more complex dynamics were also shown to arise whereby a temporary second attractor existed only during wet periods [*Peterson et al*., 2012]. Such repeated and complex switching mechanisms highlight the need to identify and locate the existing attractors (and repellors) before

exploring their emergence. To do so without first identifying the existence of the attractors would make the interpretation of the subtle and complex switching mechanisms presented within the companion paper unnecessarily challenging and weaken consequent insights. Additionally, identifying the existing attractors can inform how, say, land use change could alter the system resilience and, hence, the vulnerability to disturbances. Similar techniques to those developed herein have been used to quantify such a change of resilience due to catchment clearing [*Anderies*, 2005; *Anderies et al*., 2006], rangeland grazing [*Anderies et al*., 2002] and island formation within the everglades system [*D'Odorico et al*., 2011]. In summary, the proposed method for identifying attractors under stochastic forcing was essential for interpreting the results of the companion paper but may also be valuable to other studies quantifying the change in resilience under stochastic forcing.

For some models, identifying the existence of multiple attractors can be straightforward. Provided it is appropriate to apply mean forcing rates and the model is simple, then attractors can be identified by running the model from different initial conditions. If the simulations converge to different stable solutions, then two attractors exist. Under stochastic forcing, however, individual simulations would not converge to a stable solution due to the continued disturbance. At the end of the simulation, a distribution in the relevant hydrological output would be produced. A bimodal distribution may indicate two hydrological attractors exist but a bimodal distribution could also result from differing climatic periods or antecedent conditions and not multiple attractors. Conversely, it has been shown that a unimodal distribution can be produced when two attractors exist if the system frequently switches between the attractors [*Peterson*, 2009]. Furthermore, *Peterson et al*. [2012] and the companion paper show that the number and state space location of attractors change with the forcing. Considering that climate exerts a continuous and often significant stochastic disturbance on hydrological systems, and the hydrological response is nonlinear, identifying multiple attractors from hydrological data or model outputs is challenging and adoption of such a simple approach would be inappropriate.

When stochastic forcing has been used to identify multiple hydrological attractors all efforts known to the authors have relied upon time-integration simulations [*Guttal and Jayaprakash*, 2007, 2009] or probability density functions (PDF) of state variables derived from stochastic differential equation [*Rennermalm et al*., 2010; *Runyan and D'Odorico*, 2012, 2013; *D'Odorico et al*., 2005]. While informative, both approaches quantify the emergence of attractors, and not the existence of attractors. With regard to time-integration methods using stochastic forcing, they can be an informative means for identifying the existence of attractors, but if the switching between the attractors is very frequent then the attractors may be difficult to identify [*Guttal and Jayaprakash*, 2007]. Additionally, the forcing may never be sufficient to cause a switch to another attractor, and hence it would go undetected. With regard to PDF methods, a bimodal distribution has often been used to indicate multiple attractors emerging [*Scheffer and Carpenter*, 2003]. However, if a system spends most of its time within one attractor basin and rarely switches to a second attractor basin then a bimodal distribution may not emerge [see *Peterson*, 2009, section 6.4]. Hence, PDF methods may fail to properly identify the existence of two attractors. Both methods also suffer from an inability to distinguish between multiple attractors that exist under average forcing conditions and temporary attractors that exist only during wet or dry periods [*Peterson et al*., 2012; T. J. Peterson et al., Multiple hydrological attractors under stochastic daily forcing: 2. Can multiple attractors emerge?, submitted to *Water Resource Research*, 2013]. Furthermore, neither method can identify the repellor between the attractors or explore how the number of attractors change with a system property; for example hydraulic conductivity [*Peterson et al*., 2009] or land use [*Anderies*, 2005]. All of these weakness can be overcome using the more advanced technique of continuation analysis (which is explained below) to quantify the existence of attractors. However, to the authors knowledge, all application of continuation analysis to resilience studies, and hydrology, have used mean (often annual) forcing rates [e.g., *Anderies*, 2005; *Rennermalm et al*., 2010; *Ridolfi et al*., 2006; *Runyan and D'Odorico*, 2010; *Peterson et al*., 2009; *Guttal and Jayaprakash*, 2007; *D'Odorico et al*., 2011; *Heffernan*, 2008; *van Nes and Scheffer*, 2005]; an assumption which often required the use of a very simple model. The consequence of this is that the identification of multiple attractors may be weakened if the fluxes are estimated at an inappropriate timescale for their dynamics.

Equilibrium continuation analysis (a subset of bifurcation theory) is a powerful tool for quantifying the state space locations of attractors and repellors as a function of one model parameter. Basically, numerical equilibrium continuation analysis finds a value for each state variable at which all time derivatives are zero and then traces this state space point with a change in one model parameter. *Peterson et al*. [2009] used a type

of continuation analysis to quantify the depth to water table of the attractors and a repellor with a change in a single model parameter; which was the lateral hydraulic conductivity. However, as a result of the model's within-year periodic forcing, the soil moisture and groundwater storage state variables do not approach a time independent equilibrium but rather a sinusoidal-like repeating cycle, formally called a *limit cycle*. As the cycle results from climatic forcing rather than the system equations, it is in actual fact a *forced* limit cycle. Effectively, limit cycle continuation (LCC) traces this phase-plane with incremental changes in a parameter. Like equilibrium continuation, limit cycle continuation starts from an initial limit cycle derived from time integration of the model, and, using a predictor-corrector algorithm, increments the model parameter of interest and then uses a Newtonian method to adjust the parameter and state variables until stable phase cycles, for all state variables, are achieved. The aforementioned weakness of *Peterson et al*. [2009] using monthly mean climate forcing, rather than stochastic daily forcing, arose because the forced limit cycle continuation analysis required input of the monthly mean climate forcing. This was required in order to achieve a stable closed cycle of groundwater head and soil moisture, at all model nodes, throughout the year. This use of monthly forcing resulted in dampened soil moisture dynamics and thus a reduced peak unsaturated conductivity and recharge. Considering that the multiple attractors within *Peterson et al*. [2009] are very dependent upon recharge, it remains unclear as to whether the multiple attractors still exist under stochastic climate forcing. To overcome this limitation of continuation analysis, this paper proposes a new continuation method that allows estimation of attractors and repellors under upscaled daily stochastic forcing; effectively assessing if multiple attractors exist and hence could emerge under daily forcing. In applying this methodology, daily forcing was adopted because it was considered to be an adequate compromise between the time scale of relevant hydrological processes, the availability of climate data, and the computational requirements of the continuation analysis.

This paper is organized as follows. Section 2 details the hypothetical coupled vadose zone-hillslope Boussinesq model, new limit cycle methodology, modifications to the ecohydrological model of *Peterson et al*. [2009] and details the hypothetical investigation undertaken. Section 3 presents results for the hypothetical investigation, in which the new limit cycle methodology is assessed against time-integration estimates of the attractors. Section 3 discusses the results and the implications for the likelihood of a catchment having multiple attractors and the likelihood of them emerging under stochastic forcing; the latter being further addressed within the companion paper (Peterson et al., submitted manuscript, 2013).

2. Methodology

The ecohydrological model adopted to investigate the existence and emergence of attractors is from *Peterson et al*. [2009] and is summarized in Figure 2. It shows the model as a cross section over the catchment length with an inset summarizing the unsaturated zone component. Lateral flow occurs by surface runoff and by saturated flow within the aquifer; the flow direction of which is horizontal to the aquifer-basement boundary. Saturated lateral flow is represented by the standard Boussinesq approximations and can occur in both the *aquifer* and the soil layer if the water table is within the soil layer. The width of the catchment decreases toward the outlet and the width adopted is shown in Figure 3. Following *Troch et al*. [2003], for computational efficiency, the saturated flow across the width dimension is assumed to be parallel and is simulated without an additional spatial dimension. The depth of the unsaturated layer is the minimum of the depth to the lower soil layer boundary and the depth to the water table. With respect to the inset in Figure 2, the unsaturated zone is vertically lumped and rainfall is partitioned to interception, runoff and infiltration. Unsaturated fluxes are assumed vertical and, if the water table is within the soil layer, both recharge to and uptake from the groundwater can occur.

Central to the simulation of the positive feedback, and hence the possibility of two attractors, is the interaction between the vegetation and the saline water table. The positive feedback is summarized in Figure 4. When the water table is just intersecting the root zone and a large rainfall event occurs, the soil moisture increases and, if moist enough, produces a notable increase in recharge. The water table subsequently rises and an increased fraction of the root zone is within the water table. Because the water table is assumed to be saline, phreatic transpiration is zero and osmotic effects reduce the root-water uptake from the unsaturated zone. This is simulated by defining the leaf area index (LAI) as a logistic function of the depth to the (saline) water table. That is, a simple empirical relationship was adopted whereby the LAI approaches a

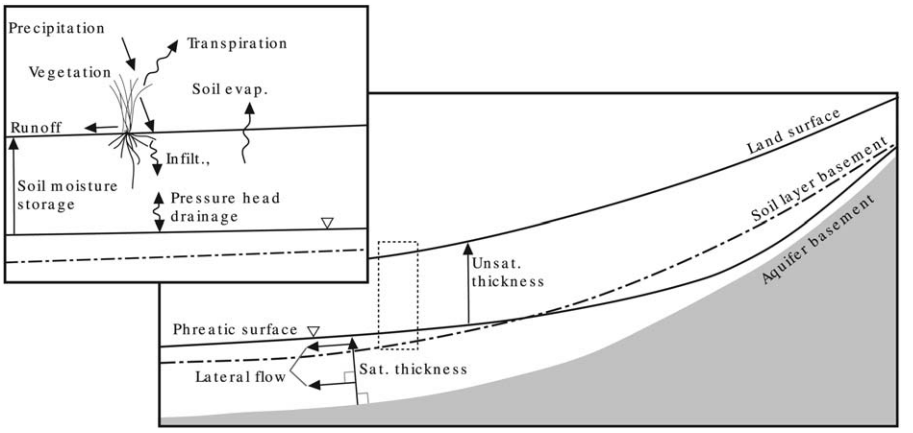

Figure 2. Schematic of the hillslope ecohydrological model. (top left) Inset details the one-dimensional unsaturated zone model. Adapted from *Peterson et al*. [2009].

maximum when the (saline) water table is far below the root zone and equals zero when the water table is at the surface. When the water table rises, the LAI declines, and transpiration also declines. This further increases the soil moisture and, during the next recharge event, further elevates the water table completing the positive feedback cycle. If this positive feedback produces a greater increase in recharge than can be discharged through increased saturated lateral flow then a shallow water table attractor can exist.

The ecohydrological model may appear overly complex for an exploration of multiple attractors. A very simple model could have been adopted, such as that of *Peterson et al*. [2012], but such models may produce two hydrological attractors only at the expense of highly implausible hydrological fluxes, storages and/or parameters [see *Peterson*, 2009, section 3.4.2, for an example of the latter]. With regard to *Peterson et al*. [2012], the weaknesses were that no lateral flow was simulated and all unsaturated fluxes were simulated using a single function; a simplification that rendered it inappropriate for simulating daily fluxes. With regard to the adopted ecohydrological model, its inclusion of saturated lateral flow and semidistributed soil moisture allowed more realistic spatial patterns and interactions to be simulated, which was considered to be a necessary complexity for meaningful insights into the emergence and existence of multiple attractors. While further complexity could have been added, for example by the addition of salt storage variables or deterministic vegetation dynamics, this would have made numerical exploration of the attractor overly burdensome for what would most likely be minimal additional insights or validity.

The investigation of multiple hydrological attractors under stochastic forcing was undertaken using the ecohydrological model, parameters and general head boundary condition of *Peterson et al*. [2009] and composed of two main steps. First, a stochastic forced limit cycle continuation algorithm was developed (henceforth, referred to as the *stochastic forced limit cycle continuation* method, or SFLCC). It was then used to quantify the depth to water table of the attractors and repellor for a range of saturated lateral conductivity (k_{sat}) rates and the following three values of maximum infiltration (I_o), with the latter effectively simulating no infiltration excess runoff: 50, 200, and 10^6 mm d^{-1}. Second, the SFLCC attractor estimates were independently estimated using time-integration simulations.

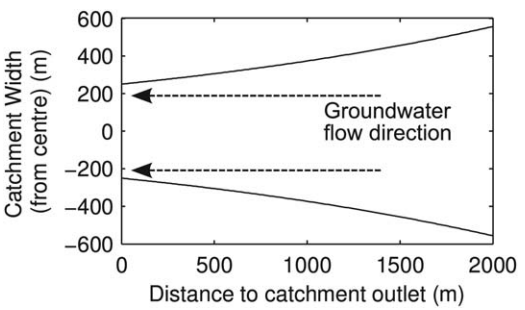

Figure 3. Plan view of the model dimensions and groundwater flow direction.

For transparency, the data and MatLab code for the model and continuation analysis are available as supplementary material to this paper. Next, the following aspects of the methodology are detailed: (i) modifications to the model of *Peterson et al*. [2009]; (ii) the input climate forcing

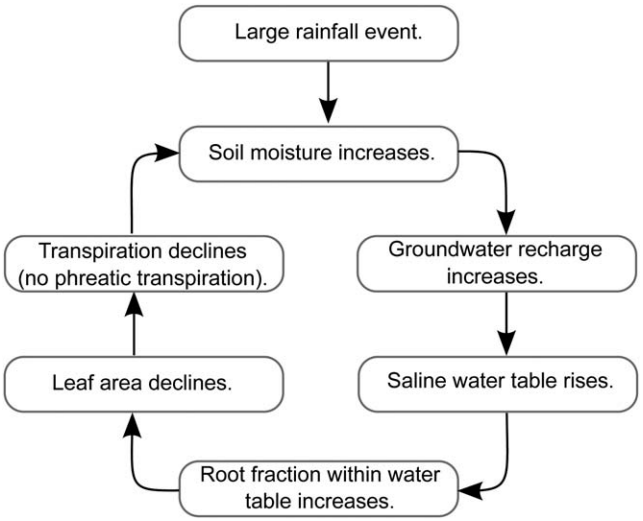

Figure 4. The positive feedback giving rise to the possibility of multiple attractors.

data; (iii) the climate upscaling methodology; (iv) identification of the attractors using SFLCC; and (v) identification of the attractors using time integration of the model.

2.1. Model Modifications

The ecohydrological model of *Peterson et al*. [2009] was modified to address minor conceptual weaknesses. Four modifications were undertaken: (i) smoothing at the soil-aquifer boundary was made independent of the catchment width; (ii) the simulation of dry cells was restructured to be consistent with Darcy's Law; (iii) the infiltration equations were restructured in order to better simulate infiltration excess runoff; and (iv) the parameters for vegetation wilting and stress points were converted from units of volumetric soil moisture to soil water pressure (this modification would not change the model results). Each modification is detailed within Appendix 6. The most significant was the modification to the equation for infiltration. This was required because, in *Peterson et al*. [2009], the threshold smoothing function for the infiltration rate incorrectly estimated a negative infiltration rate during high rainfall events when the soil moisture deficit approached zero. Modifying the smoothing equation to eliminate this error resulted in a considerable expansion in the range of saturated lateral hydraulic conductivity values predicted to have two attractors compared with that of *Peterson et al*. [2009]. A second notable modification addressed the simulation of dry groundwater cells. A theoretically rigorous and, to the authors knowledge, novel variant of Darcy's Law was derived to simulate lateral flow within an aquifer of smoothly declining hydraulic conductivity with depth. This, for example, facilitates efficient simulation of flow within an aquifer of declining weathering with depth, and presumably hydraulic conductivity, using a single layer model.

2.2. Climatic Forcing Data

Following *Peterson* [2009] and *Peterson et al*. [2009], the climate data composed of daily rainfall and daily FAO56 reference evapotranspiration (ETo) obtain from SILO for 143.45° longitude and −37.10° latitude [*Jeffrey et al*., 2001]. These coordinates approximate the daily rainfall gauge 081000 and are for the town of Avoca, Victoria Australia; at which daily rainfall records exists from 1884 to the present. The mean annual rainfall and ETo are 541.7 and 1103 mm yr−1, respectively, and a summary of the monthly forcing is presented in Figure 5. The use of observed climate forcing, rather than theoretical forcing, was adopted to ensure that realistic longer term structure (e.g., interannual and interdecadal) was incorporated into the forcing. This was viewed as important given the potentially long memory of groundwater systems (which results from a large storage capacity and a slow drainage rate), and could not have been achieved using simple Poisson rainfall event and exponential rainfall depth distributions as adopted by *Eagleson* [1978], *Laio et al*. [2001], and *D'Odorico et al*. [2005]. The longer term structure was, however, only relevant for the stochastic daily simulations undertaken within the companion paper. The climate scaling undertaken within this paper aggregates all data for given month, causing these longer term structures to be omitted.

2.3. Climate Scaling

The estimation of attractors and repellors using limit cycle continuation analysis requires the within-year climate forcing to be a smooth closed loop of nonstochastic monthly averages. This is required as limit cycle continuation solves a boundary value problem using a dynamic set of time points within the annual cycle and not points fixed in time. To meet this requirement, *Peterson* [2009] and *Peterson et al*. [2009] used sinusoidal curves fitted to the mean monthly precipitation and ETo; however, this failed to account for the nonlinear relationship between precipitation intensity and infiltration emergent at finer timescales. To take

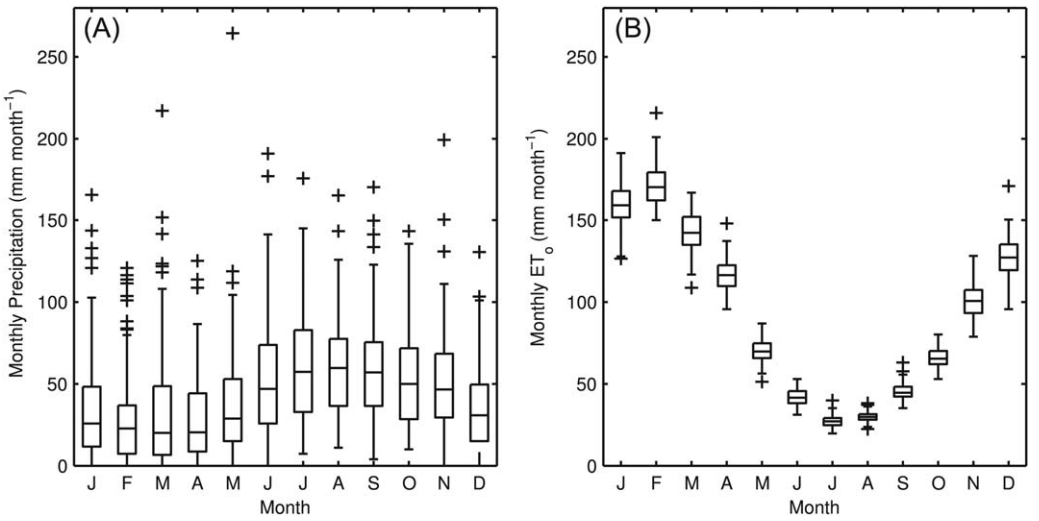

Figure 5. Box plots of monthly climate data as obtained from SILO [*Jeffrey et al*., 2001] at 143.45° longitude and −37.10° latitude. (a) Monthly precipitation. (b) Monthly potential evaporation.

account of this nonlinear process, stochastic daily forcing was incorporated into the continuation analysis by upscaling daily forcing to monthly using an extension of the empirical cumulative distribution function (CDF) methodology of *Kandel et al*. [2005].

To illustrate the upscaling methodology, Figure 6 summarizes the four steps undertaken. In step one, the daily precipitation from all years for a given month were collated and the daily precipitation at a range of percentiles from 0 to 100 was calculated. This was repeated for all months of the year and daily PET was analyzed similarly. Step 1 of Figure 6 shows the observed monthly precipitation and PET at 11 percentiles. For each percentile of precipitation and PET, a cubic Hermite spline was then fit across the 13 months from December to December. In applying this step, an equal number of percentiles was chosen for precipitation and PET, ranging from 0 to 100. These were heavily skewed toward the upper percentiles in order to adequately characterize extreme precipitation events. Hermite splines were chosen over traditional cubic splines as they were found to eliminate negative estimates.

In step two, the splines were prepared for input to the ecohydrological model. For any point in the year, the splines enabled a CDF for precipitation and PET to be derived. To illustrate, step 1 within Figure 6 shows 11 percentiles derived from the climate record and the splines fitted to each month of a single percentile. Each spline was then interpolated to obtain a precipitation rate for the 20th of July. In step 2 of Figure 6, these interpolated values were combined to produce a CDF of precipitation for the 20th of July. The interpolated 99th percentile is shown in both the yearly plots and CDF plots of Figure 6.

In step 3, the interpolated climate CDFs were used within the ecohydrological model. For a given percentile of climate forcing, each model flux was calculated. This was repeated for all percentiles, with all percentiles using the same state-variable values, to produce a CDF for each model flux. Here it was assumed that the precipitation and PET had a perfect negative rank correlation.

In step 4, the state-variable values and the fluxes at a given percentile were input to the model differential equations to give the rate of change in the model state variables. This was repeated for all percentiles to produce a CDF for rate of change in the groundwater storage and soil moisture storage at each model grid cell. By numerically integrating, these rate of change CDFs from percentiles 0 to 100, the expected or mean rate of change in each model state variable at each grid cell was obtained. This rate of change could then be used within the limit cycle continuation analysis or time integration of the model. Importantly, the CDF integration required the assumption that the omission of antecedent conditions from within a month does not cause a significant change in the model fluxes or the rate of change.

In implementing this upscaling, an adequate number of percentiles was determined by comparing the numerically integrated monthly forcing against the observed mean monthly forcing. In this investigation,

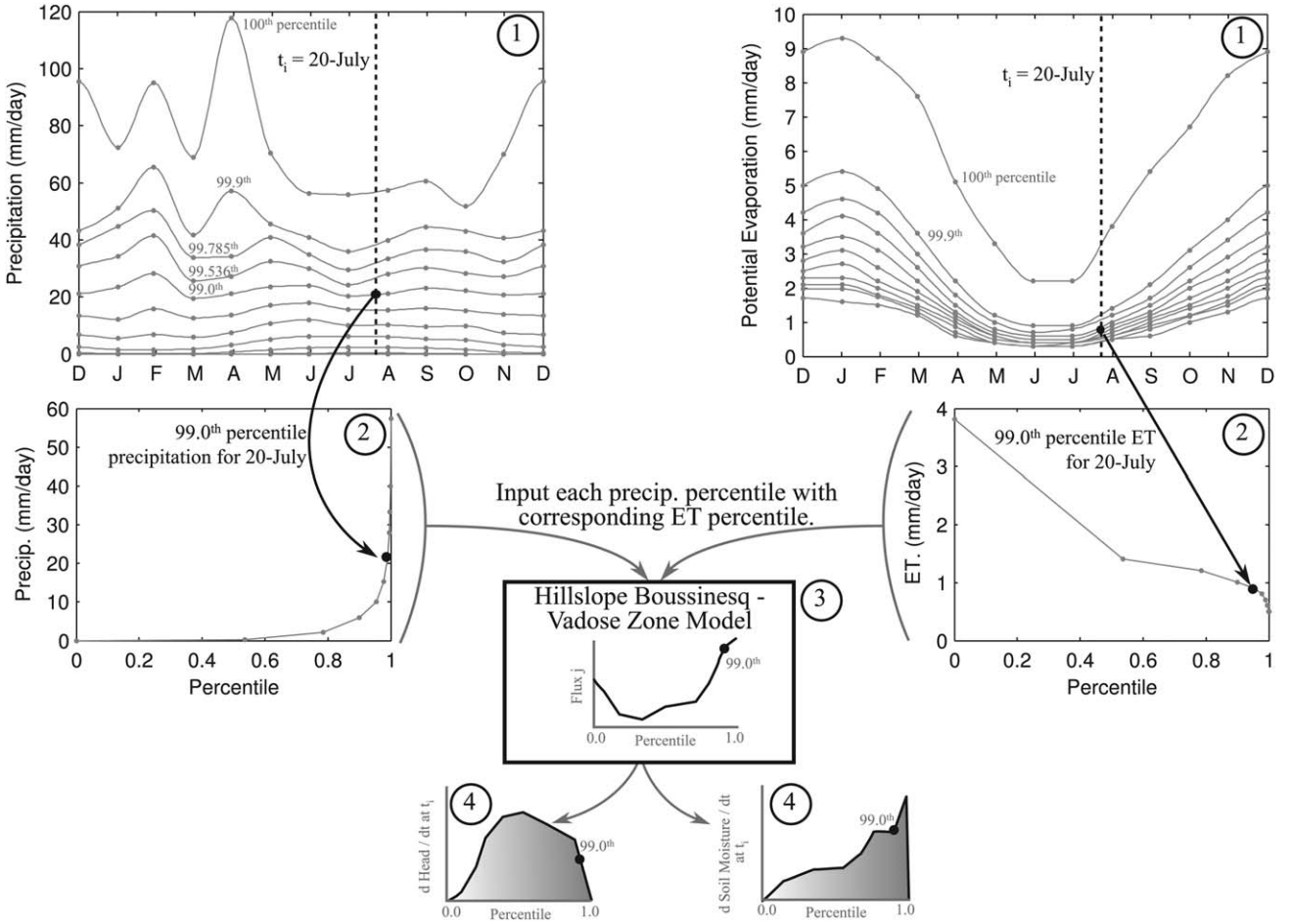

Figure 6. Example of the climate upscaling methodology. (1) denotes 11 percentiles of monthly precipitation and ET and the cubic Hermite spline; (2) presents the cumulative distribution functions (CDF) for 20 July derived from the fitted splines; (3) illustrates that each of the 11 climate forcing percentiles for 20 July are input to the model to produce a CDF for each flux; and (4) illustrates that the flux CDFs are summed to produce CDFs for the rate of change in the two state variables, which are then numerically integrated to produce a nonprobabilistic rate of change for the state variables.

50 log-spaced probabilities were adequate (with points concentrated near the 100th percentile). Clearly, the use of upscaled climatic forcing cannot be assumed to produce identical results to that from daily time step forcing because the upscaled forcing ignores within-month antecedent variations. To assess this, time-integration solutions were conducted with and without the upscaling for a range of the saturated lateral conductivity parameter values. For the simulations with upscaled forcing, the above upscaling method was undertaken using only the daily forcing for a given month of a given year, rather than the daily data for a given month from all years. The upscaled simulated depth to water table was found to be effectively indistinguishable from the nonupscaled simulations (results are not presented). Finally, the upscaling, when undertaken for limit cycle continuation, also aggregates the forcing data over all years for a given month to a single CDF for precipitation and PET. This averages over interannual variability in climate and interannual antecedent conditions and thus their effect is also averaged.

2.4. Limit Cycle Continuation Detection of Attractors and Repellor

The SFLCC was undertaken for the saturated lateral conductivity parameter, $k_{s_{max}}$. It was undertaken using MATCONT-CL [*Dhooge et al*., 2003] with the following modifications: (i) a center weighted finite difference Jacobian (note, an adaptive finite difference step size [*Ridders*, 1982] was implemented but trials found it to be unnecessary); (ii) Gauss-Newton line-search optimization was used [see *Press et al*., 2007, section 9.7.1]; and (iii) the boundary value problem (BVP) collocation scheme for the convergence of the model was modified for periodicity resulting from seasonal climate forcing and not the differential equations. The

continuation started from $k_{s_{max}}$ of 5 m d^{-1} and the deep depth to water table attractor. The BVP was solved with 12 solution nodes and five collocation points between each node; maximum step length of 1000 (dimensionless); and a normal vector tolerance for the Newton's residual and function error of $1E-6$ and $1E-4$, respectively. The LCC was undertaken both with and without the climate upscaling for each of the three I_o values. For the upscaled continuation, or SFLCC, the entire input climate record was used to derive the upscaling empirical CDFs.

2.5. Time-Integration Estimation of Attractors

To provide an estimate of the attractors, independent of the SFLCC algorithm, time-integration solutions were derived using the upscaled climate forcing for a range of $k_{s_{max}}$ values at each of the three I_o values. An attractor estimate (but not a repellor estimate) could be derived using time integration because, under non-stochastic forcing, if a system converges over time to different attractors from different initial conditions then multiple attractors are likely to exist [see *Peterson et al.*, 2012, for an example]. Herein, the state space locations of attractors were estimated by time integration from two water table initial conditions of 90% and 40% of the maximum saturated thickness (i.e., shallow and deep, respectively) and for $k_{s_{max}}$ values from 0.1 to 1.4 m d^{-1} at increments of 0.1 m d^{-1}. The nonlinear PDE of the ecohydrological model was solved using the MatLab variable time step solver *ode15s* [*Shampine and Reichelt*, 1997] modified so that the solver completed estimation for a given month exactly at the end of the month. This ensured the CDF of daily climate forcing for a given month was not inadvertently used for the first time step of the following month. Simulation duration was 1000 years and the adequacy of this duration for convergence to a stable solution was assessed by inspection of phase-cycles from selected simulations. To summarize the simulations, the depth to water table throughout the final year of simulation was then extracted and plotted against $k_{s_{max}}$. Considering that the numerical methods for the time integration were significantly simpler than those for SFLCC, the time-integration solutions were taken as a benchmark against which the SFLCC results were assessed.

3. Results

Figure 7 details the limit cycle continuation results at 250 and 1000 m from the catchment outlet for the three maximum infiltration, I_o, parameter values of 50, 200, and 10^6 mm d^{-1}. Similar results for soil moisture are not shown. Each plot details the LCC estimated attractor and repellor depth to water table against the saturated lateral conductivity, $k_{s_{max}}$, for both monthly average climate forcing and the upscaled forcing. To independently assess the upscaled attractor estimates, each plot also details the time-integration solutions using upscaled forcing from a shallow and deep initial condition at 14 values of $k_{s_{max}}$. Four key findings emerge from Figure 7 and each is discussed below.

Two attractors existed at all model locations under both monthly and upscaled daily forcing. With regard to the LCC upscaled forcing results at 250 m, when $k_{s_{max}}$ was less than 0.25 m d^{-1}, the shallow water table attractor was 0.5 m below the land surface and within the soil layer; which was 2.4 m thick at 250 m from the outlet. As $k_{s_{max}}$ increased toward the upper fold-point, the water table lowered to approximately 1.25 m below the land surface (note, the fold-points are the upper most $k_{s_{max}}$ value at which the shallow attractor exists and the lower most $k_{s_{max}}$ value at which the deep attractor exists). Conversely, for the deep attractor, as $k_{s_{max}}$ approached the left fold point the water table was approximately 2.25 m below the land surface. As $k_{s_{max}}$ increased, the deep attractor lowered slightly to a depth of 2.6 m below the land surface, or 0.16 m below the soil layer. At 1000 m, two attractors existed despite the water table being 5–10 m below the soil layer. Considering that the root-zone extended throughout the soil layer, only in the lower catchment was the water table sufficiently shallow to interact with the vegetation and cause a positive feedback. When the feedback was sufficiently strong to produce a shallow attractor, the shallow attractor propagated from the lower to the upper catchment. Hence, multiple attractors existed at all model locations but existed because of the aquifer-vegetation interact within the lower catchment.

The $k_{s_{max}}$ range with two attractors (i.e., the difference between the fold-points) was constant throughout the catchment and was independent of I_o. However, the two attractor range did shift to higher values of $k_{s_{max}}$ as I_o increased. Hydrologically, an increased maximum infiltration rate shifted the shallow attractor to higher saturated lateral conductivities because less runoff and more infiltration occurred on days of high rainfall. This increased the soil moisture and hence the groundwater recharge. For the case of $I_o = 50$ mm

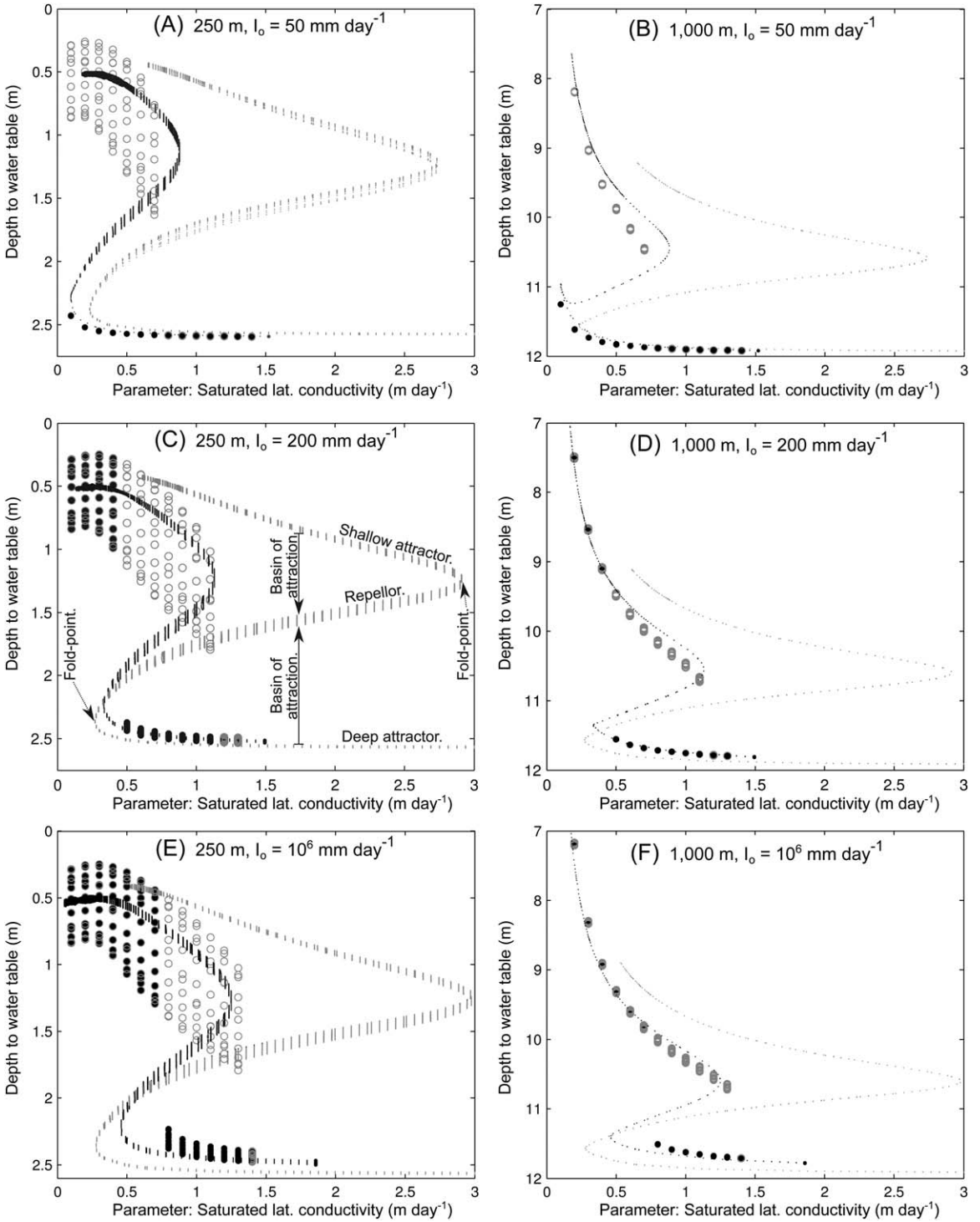

Figure 7. Time integration and forced limit cycle continuation results at 250 m (a, c, and e) and 1000 m (b, d, and f) from the catchment outlet for a max infiltration rate, I_o, of 50, 200, and 10^6 mm d^{-1} (a and b, c and d, and e and f, respectively). The continuation results from the upscaled forcing (SFLCC) are denoted by black bar. The continuation results from the mean monthly forcing (i.e., not upscaled) are denoted by gray bar. The time-integration estimates of attractors are denoted by circle for those simulations from the shallow initial condition and filled circle for those from the deep initial condition. Depths from the time-integration simulations for each month of the year are also shown. The upper and lower series of bar points are the attractors and the series of bar values centered between the attractors is the repellor. Importantly, each single bar also denotes the annual range in depth to water table resulting from the seasonal forcing. If magnified, each can be seen to composed of many dots. These dots are the within-year points of the annual phase space and are determined by the limit cycle continuation algorithm. When plotted with soil moisture a closed-loop is formed as shown within Figure 8(a) of *Peterson et al*. [2009].

d^{-1}, when $k_{s_{max}} = 1$ m d^{-1} and the water table is shallow, the recharge is less than the aquifer drainage rate. Hence the shallow attractor does not exist. However, when I_o increases to 200 mm d^{-1} the additional recharge cannot be discharged by the aquifer and the shallow state exists when $k_{s_{max}} = 1$ m d^{-1}.

The $k_{s_{max}}$ two-attractor range significantly contracted under upscaled forcing compared with that under monthly forcing. This occurred for all values of I_o and at all locations within the catchment. The contraction occurred predominately because the upper $k_{s_{max}}$ fold-point shifted to a lower value of $k_{s_{max}}$. That is, under upscaled forcing, the shallow attractor had a reduced parameter range. This indicates that under daily climate forcing, relative to using monthly forcing, fewer catchments appear to have multiple attractors. Hence, more catchments appear to be resilient to climatic disturbances because they have only one attractor. This change in attractors occurred because, under upscaled forcing, the episodic nature of rainfall and its nonlinear propagation through the vadose zone was better captured. Upscaled forcing led to increased runoff, resulting in lower soil moisture than under monthly forcing. As vertical unsaturated hydraulic conductivity was very nonlinearly dependent upon soil moisture, this then produced a large reduction in recharge. Hence, the shallow attractor could not exist at a high a value of $k_{s_{max}}$, resulting in the existence of only the deep attractor.

The time-integration solutions shown in Figure 7 were derived using significantly simpler numerical methods than those for the SFLCC. Furthermore, the time-integration solutions for a number of $k_{s_{max}}$ values and initial depth to water table values were plotted against time and confirmed to have converged to a stable solution (plots not shown). Hence, the time-integration solutions are considered a reliable measure of the attractors and provide a means for assessing the reliability of the SFLCC. With regard to the SFLCC results, at 1000 m from the outlet, the two-attractor $k_{s_{max}}$ range, parameter location and the depth to water table at which they exist was reliably estimated. The only consistent discrepancy was the depth to water table of the shallow attractor from the time integration being slightly deeper than from SFLCC. At 250 m from the outlet the two-attractor $k_{s_{max}}$ range and parameter location and the depth to water table at which they exist was less reliably estimated by the SFLCC. Specifically, for I_o of 200 and 10^6 mm d^{-1} (Figures 7c and 7e) the lower fold-point at $k_{s_{max}}$ of 0.5 m d^{-1} was underestimated by SFLCC. Also, and most significantly, the seasonal variation in depth to water table (as denoted within Figure 7 by the *y* axis range of each | symbol of the LCC results) differed significantly between the two methods. At the shallow attractor, the time-integration method estimated a seasonal variation in depth to water table of about three quarters of 1 m for any $k_{s_{max}}$ value, while SFLCC estimated a range of only about 10 cm. At the deep attractor the estimates of seasonal variation were comparable.

In exploring this difference in within-year variability, a likely cause was a model modification undertaken to increase the numerical stability of the continuation analysis. From equation (26) of *Peterson et al.* [2009], the net lateral saturated flux term within the PDE was multiplied by $\frac{1}{\left(1-\lambda\frac{\theta}{\phi}\right)}$, where λ is a dimensionless variable for the fraction of the soil layer that is saturated by the water table; θ is the dimensionless soil moisture fraction; and ϕ is a dimensionless parameter for the soil porosity. With regard to the modification, and as discussed within paragraph 30 of *Peterson et al.* [2009], when the water table is near to the land surface and the soil is near to saturation the above scaling function approaches infinity. This causes the rate of change in the groundwater storage to approach infinity and a singularity to emerge. This singularity caused the continuation analysis to fail when $k_{s_{max}}$ was low and when tracing the shallow attractor. To produce a solution over a wide range of $k_{s_{max}}$, the saturated fraction, θ/ϕ, was multiplied by a constant of 0.5, only during the continuation analysis. This eliminated the possibility of a singularity and allowed reliable continuation analysis. To investigate if this modification was the cause of the low within-year variability, the SFLCC was repeated with this singularity constant increased from 0.5 to 0.9 and 1.0. Figure 8 shows results for I_o of 200 mm d^{-1} at 250 m from the outlet. It shows that even for a singularity constant of 1.0 the within-year water table variability does not approach that of the time-integration solutions. The only notable increase in the within-year variability was at the repellor. Furthermore, it also shows that as the constant increases from 0.5 the continuation analysis terminates at lower values of $k_{s_{max}}$. Hence, the low within-year variability from the continuation analysis was not caused by the aforementioned model modification and the cause remains unresolved.

Overall, and considering that the purpose of the continuation analysis was the estimation of the number of attractors and the repellor depth to water table (for use in the companion paper), the SFLCC did prove reliable. However, with regard to the use of the repellor estimates within the companion paper, the seasonal range in the depth to water table appears to have been underestimated within the lower catchment.

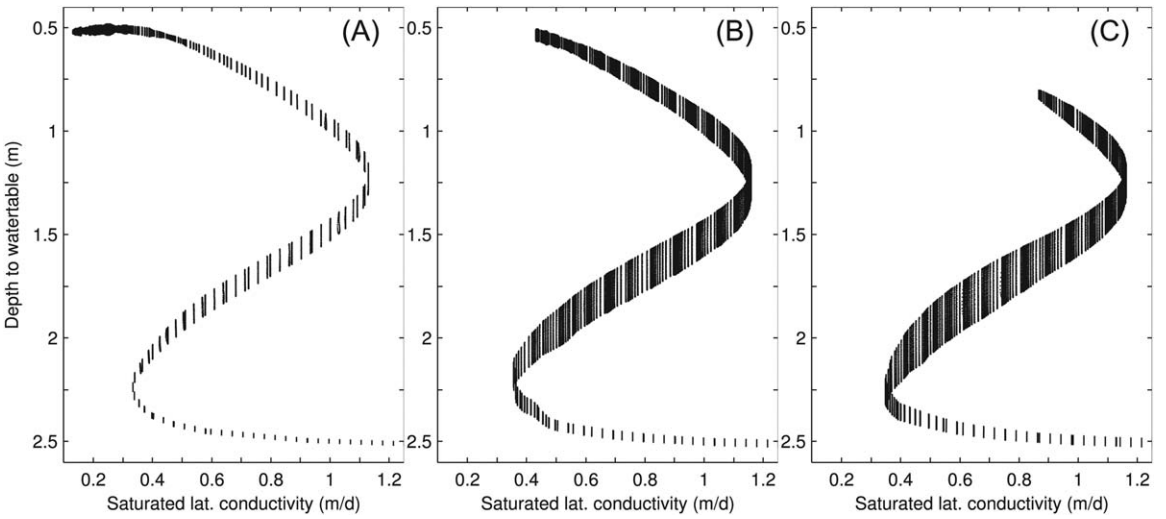

Figure 8. *Forced* limit cycle continuation results for three values of the singularity constant. All plots are for 250 m from the catchment outlet, a maximum infiltration, I_o, of 200 mm d^{-1} and the symbols are as for Figure 3. Importantly, setting the singularity constant to one (that is, allowing a singularity to emerge within the model equations) did not result in within-year depth to water table fluctuations comparable to those from the time integration (see Figure 3c). (a) Singularity constant of 0.5. (b) Singularity constant of 0.9. (c) Singularity constant of 1.0.

4. Discussion and Conclusions

This paper explored if multiple hydrological attractors can exist within a hill slope-vegetation model under daily stochastic forcing. Previous efforts to identify hydrological attractors have been limited to nonstochastic monthly or annual climate forcing. The motivation for this exploration was that, if theories of hydrological systems having more than one attractor are to advance beyond modeling studies to the identification of multiple attractors in the field, it first needs to be ascertained if multiple attractors can exist within models under stochastic daily forcing.

The investigation was undertaken using a hillslope ecohydrological model [an extension of *Peterson et al.*, 2009] that had a positive feedback resulting from the interaction of vegetation with a saline water table. To identify the attractors, a limit cycle continuation climate scaling technique was developed that represented the nonlinear effects of stochastic forcing through the model. Using the technique, the depth to water table of attractors were identified over a range of saturated lateral conductivity, $k_{s_{max}}$, values and at three values of maximum infiltration, I_o. As shown in Figure 7, multiple hydrological attractors were found to exist under daily forcing over a limited range of $k_{s_{max}}$ values. Most significantly the timescale of the stochastic forcing was found to be critical because, in comparison to using mean monthly climate forcing, the use of daily climate forcing significantly reduced the $k_{s_{max}}$ range of two attractors. This reduced two-attractor range suggests that fewer catchments may have multiple attractors than was predicted by use of monthly climate. Hence, more catchments appear to be resilient to climatic disturbances because they have only one attractor.

With regard to the maximum infiltration rate, I_o, the $k_{s_{max}}$ range with two attractors was independent of I_o but did shift to higher values of $k_{s_{max}}$. These findings were well supported by time-integration simulations also using the climate upscaling technique. Considering that the shallow attractor always existed at very low values of $k_{s_{max}}$, this indicates that those catchments most likely to have at least the shallow attractor are those having a low transmissivity and a high limiting infiltration rate.

The comparison between the two attractor estimation methods (i.e., SFLCC and time-integration methods) indicated that the within-year head variability at the shallow attractor in the lower catchment was underestimated by the SFLCC. This was hypothesized to be due to a model modification undertaken to increase the numerical stability of the continuation analysis. However, trials undertaken without this modification showed it not to be the cause of the reduced head variability. An alternative hypothesis is that limit cycle continuation used too few within-year time points to characterize the annual phase cycle. That is, continuation analysis used only 45 time points while time integration used a large and varying number of points as

defined by a variable time step differential equation solver. While this inconsistency between the attractor estimation methods is not expected to influence the repellor estimates, and hence the validity of their use within the companion paper, this issue does require further research.

This paper investigated the possible existence of multiple attractors. However, the two methods developed to identify the attractors both relied on the same climate upscaling method applied to the same hypothetical model. Regarding the climate, the two methods developed to identify the attractors both used a climate scaling approach whereby daily rainfall variability was simulated using CDFs. It was assumed that the same CDF was applicable for every year and all of the daily climate record was used to construct distributions of daily forcing for each calendar month. Hence, each month included all of the historic extreme climate events and, while these events are rare, the monthly CDF has a higher variability than is likely within any given month of a year. Additionally, in the construction of the monthly CDFs, the serial correlation between the climate events and interannual variability were ignored. The significance of interannual climate variability on ecohydrological attractors was investigated by *Runyan and D'Odorico* [2012] and *Runyan and D'Odorico* [2013] and, while both studies investigated the emergence and not the existence of multiple attractors, interannual climate variability did significantly influence the switching between attractors. The significance of interannual climate variability for the existence of multiple attractors is, however, a more challenging question. One possible method for addressing it would be to undertake the limit cycle continuation at the timescale of the interannual climate cycles, rather than at a monthly time step. This would require the interannual climate cycles to be quantified and the climate scaling to be undertaken using all years of data (not months) at a given year within the interannual cycle. It would also only be feasible if the climate cycles were dominated by a fixed timescale. In light of all this, and considering that a switch from the shallow to the deep attractor would require a long period of low rainfall while a switch to the shallow attractor would require only a shorter period of high rainfall, it is quite possible that attractors identified to exist by SFLCC may never actually emerge under real forcing. In other words, the emergence of attractors may be very different from the existence of attractors. In the companion paper, the emergence of attractors is investigated.

Both methods developed to identify the attractors also used the same simple hypothetical model. Obviously any hydrological model is a simplification of reality, but simplifications influencing the strength or existence of the positive feedback could be critical to the finding that multiple attractors can exist under daily forcing. The most pertinent of the simplifications are the omission of salt transport from the aquifer and vadose zone, the vertical integration of the vadose zone and the adoption of an empirical function for the vegetation-aquifer dynamics. Clearly, more complex approaches could be adopted that may indicate it to be highly unlikely that catchments can have multiple attractors. For example, the deterministic simulation of vegetation response to changes in the soil and/or aquifer salinity, or soil moisture and depth to water table respectively, could produce a more plastic vegetation response to disturbances that may eliminate the positive feedback or reduce its strength, and hence reduce the likelihood of catchments having two attractors. However, if multiple attractors continued to exist then the theory of multiple attractors would be strengthened. This paper adopted a similar approach whereby the realism of the forcing was increased in an attempt to falsify this theory but multiple attractors did continue to exist. Considering the numerical complexity required to identify the attractors under stochastic forcing, future efforts to falsify this theory using a more complex model may be hampered by the complexity of the continuation analysis. Therefore, in light of the findings from this and the companion paper, future efforts may best be placed in field studies to identify catchments switching between multiple attractors, which would falsify the widely adopted theory that catchments have only one attractor.

In closing, two attractors do appear to exist under stochastic forcing for a range of $k_{s_{max}}$ values. The ecohydrological model does, however, have many more parameters. Using the accompanying SFLCC code, other model parameters, boundary conditions, and spatial heterogeneity could be further explored to obtain a richer understanding of the biophysical processes resulting in multiple attractors. Furthermore, the scaling approach for inclusion of stochastic forcing within continuation analysis is likely to have wider applicability to resilience science, particularly to applications where the forcing is an inherent component of the system, as in hydrology, and not an auxiliary component not essential for system function. Additionally, there are a considerable number of hydrological models built without consideration of positive feedback or multiple attractors. Considering that most of these models require stochastic forcing, the techniques presented within this paper could be applied to identify previously unknown, or unintended, multiple attractors in these models.

Appendix A: Model Modifications

The following sections detail the four modifications undertaken to the model of *Peterson et al*. [2009].

A1. Soil-Aquifer Boundary Smoothing

Within *Peterson et al*. [2009], the boundary between the soil and aquifer layer was smoothed to facilitate numerical limit cycle continuation. However, the smoothing was noted to be dependent upon the catchment width. Within *Peterson et al*. [2009], the parameter λ_S for the smoothing had units of groundwater storage per unit of catchment length. Herein, the smoothing was made independent of the catchment width by making λ_S a function of catchment width. Specifically, the smoothing function from *Peterson et al*. [2009]:

$$\lambda = \frac{1}{1+e^{\frac{S-Saq}{\lambda_S}}} \tag{1}$$

was modified too

$$\lambda = \frac{1}{1+e^{\frac{S-Saq}{w\lambda_S}}} \tag{2}$$

where λ_S is the smoothing parameter, S [L^2] is the groundwater storage, S_{aq} [L^2] is a constant vector for the aquifer storage capacity, and w [L] is the catchment width at location x [L]. For this paper, λ_S was 0.1 m.

A2. Depth Dependent Lateral Hydraulic Conductivity

Within *Peterson et al*. [2009], the aquifer hydraulic conductivity, k_s, was modeled to decline from $k_{s_{max}}$ to zero as the saturated thickness, b [L], approached zero:

$$k_s = k_{s_{max}} \frac{b^\tau}{b^\tau + b_{k/2}^\tau} \tag{3}$$

Specifically, at a saturated thickness of $b_{k/2}$ [L] the saturated conductivity is half the maximum, $k_{s_{max}}$ [$L\ T^{-1}$], and declines at a rate τ with the saturated thickness. This was undertaken to ensure that the saturated thickness at all nodes was greater than zero without the requirement for an additional state variable vector, as used in ModFlow [*Harbaugh et al*., 2000], for the rewetting of dry nodes. This estimate of k_s was then inserted into Darcy's Law and therefore effectively assumed that this point value of k_s was representative of the entire saturated column. At values of b at which k_s rapidly declines, this method implicitly assumed the value of k_s at the phreatic surface declined far more rapidly than implied by the logistic decay function of equation (3). Herein, an approach adhering to Darcy's Law was developed. Additionally, the method developed allows simulation of lateral flow with a single model layer where the hydraulic conductivity changes smoothly with depth.

To modify equation (3), first consider that Darcy's Law for a unit width saturated lateral flow, q [$L^2\ T^{-1}$], over the saturated thickness can be rewritten as the following integral when the lateral hydraulic conductivity is uniform from the aquifer basement to the saturated thickness, B:

$$\begin{aligned} q &= bk_s \frac{\partial h}{\partial x} \\ &= \int_0^B k_s \frac{\partial h}{\partial x} db \end{aligned} \tag{4}$$

Substituting in equation (3) for k_s and moving terms independent of b to outside the integral results in:

$$q = k_{s_{max}} \frac{\partial h}{\partial x} \int_0^b \frac{b^\tau}{b^\tau + b_{k/2}^\tau} db \tag{5}$$

Solving the integral produces the following analytical version of Darcy's Law when the point value lateral saturated conductivity declines with depth below the surface at a rate of τ and, at a height of $b_{k/2}$ above the basement, equals 50% of $k_{s_{max}}$:

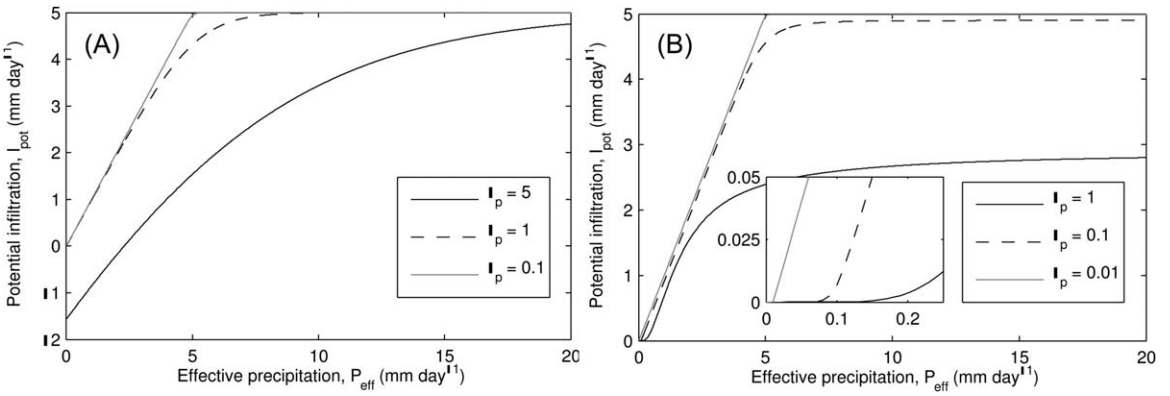

Figure 9. Example potential infiltration rates using (a) equation (3) from *Peterson et al*. [2009] and (b) the revised form (equation (10)). The soil moisture deficit was set to 5 mm and the unit of the smoothing parameter λ_p is mm d^{-1}. (a) Potential infiltration rates (equation (9)) used within *Peterson et al*. [2009]. It shows the erroneous negative potential infiltration when $\lambda_p = 5$ mm d^{-1}. (b) Revised potential infiltration rates (equation (10)). It shows λ_p should be approximately 0.01 mm d^{-1} for potential infiltration to approach the soil moisture deficit. The inset shows the threshold smoothing as P_{eff} approaches 0 mm d^{-1}.

$$q = k_{s_{max}} \frac{\partial h}{\partial x} \frac{\tau}{b} \left[\ln\left(1 + e^{\frac{b_{k/2} - b}{\tau}}\right) - \ln e^{\frac{b_{k/2} - b}{\tau}} + C \right]_0^b \tag{6}$$

By assuming q equals zero when b equals zero, the integration constant C can be derived and the following analytical equation results:

$$q = k_{s_{max}} \frac{\partial h}{\partial x} \frac{\tau}{b} \left[\ln\left(1 + e^{\frac{b_{k/2} - b}{\tau}}\right) - \ln e^{\frac{b_{k/2} - b}{\tau}} - \ln\left(1 + e^{\frac{b_{k/2}}{\tau}}\right) + \ln e^{\frac{b_{k/2}}{\tau}} \right] \tag{7}$$

Finally, the parameter τ was replaced by $1/\tau$. This was undertaken to make the smoothing more logical; that is, a larger value produces more smoothing and vice versa. For this application, the parameters $b_{k/2}$ and τ were set to 2 m and 4, respectively

$$q = \frac{k_{s_{max}}}{\tau b} \frac{\partial h}{\partial x} \left[\ln\left(1 + e^{\tau\left(b_{k/2} - b\right)}\right) - \ln e^{\tau\left(b_{k/2} - b\right)} - \ln\left(1 + e^{\tau b_{k/2}}\right) + \ln e^{\tau b_{k/2}} \right] \tag{8}$$

A3. Infiltration Potential

Peterson et al. [2009] simulated infiltration and saturation excess runoff. The actual infiltration rate, henceforth the infiltration potential P_{infilt} [$L\ T^{-1}$], was limited to the minimum of the effective precipitation, P_{eff} [$L\ T^{-1}$], and the soil moisture deficit. Within *Peterson et al*. [2009], P_{infilt} was estimated as follows, where the second equation removes the discontinuity arising from the *min* term:

$$\begin{aligned} P_{infilt} &= \min\left(P_{eff}, m_{max} - m\right) \\ &\approx P_{eff} - \lambda_P \ln\left[e^{\frac{P_{eff} - (m_{max} - m)}{\lambda_P}} + 1 \right] \end{aligned} \tag{9}$$

Here λ_P [L] is a smoothing parameter for approximating the *min* function [*Kavetski and Kuczera*, 2007], trials for which identified acceptable smoothing to occur when $\lambda_P = 0.005$ meters; m [L] is a state variable for the soil moisture storage; and m_{max} [L] is a derived variable for the maximum soil moisture capacity.

Two modifications were undertaken to equation (9). First, the infiltration smoothening parameter λ_P was reduced from $5E-3$ to $1E-5$ m. This change was required because preliminary time-integration simulations under stochastic forcing showed that, during high rainfall events when the soil moisture deficit approached zero, the smoothing component of equation (9) incorrectly estimated negative infiltration.

This outcome is illustrated in Figure 9a. Increasing the sharpness of the smoothed threshold by reducing λ_P to $1E-5$ ensured the infiltration was simulated as intended and always positive. With respect to the two-dimensional continuation plot of *Peterson et al*. [2009, Figure 8e], this modification resulted in a considerable expansion of the hydraulic conductivity, $k_{s_{max}}$, two-attractor range from 0.2 to 0.61 m d^{-1} to a range of 0.2 to 1.67 m d^{-1}.

The second modification composed of smoothing the discontinuity at zero millimeters effective precipitation (see Figure 9a). This was undertaken because it caused considerable numerical instabilities within the stochastic limit cycle continuation algorithm. It was derived from equation (4.11) of *Peterson* [2009] for smoothing soil moisture between the residual and stress point soil moisture. The form detailed below smooths P_{infilt} as P_{eff} approaches either zero or the soil moisture deficit. Figure 9b illustrates this smoothing and the insert highlights that the smoothing rate is a function of P_{eff} such that the smoothing is very rapid as P_{eff} approaches zero

$$P_{infilt} = \lambda_P P_{eff} \ln \left[\frac{1+\exp\left(\frac{P_{eff}-\lambda_P}{\lambda_P P_{eff}}\right)}{1+\exp\left(\frac{P_{eff}-(m_{max}-m)}{\lambda_P P_{eff}}\right)} \right] \tag{10}$$

A4. Transpiration Wilting and Stomata Closure Thresholds

The parameters within *Peterson et al*. [2009] for vegetation volumetric soil moisture wilting and stress, θ_{wp} and θ_*, respectively, where generalized to soil moisture pressures. This ensured that if parameters for the soil porosity, air-entry pressure or pore-size index were varied during, say, calibration then the vegetation wilting and stress soil moistures would change accordingly. To implement this, θ_{wp} and θ_* were estimated from the following rearrangement of the soil moisture retention equation of *van Genuchten* [1980]:

$$\theta_\psi = (\phi - \theta_r)\left[\frac{1}{1+\left(\frac{\psi}{\psi_a}\right)^n}\right]^m + \theta_r \tag{11}$$

where ψ [*L*] is the suction in meters of water at the wilting point or vegetation stress point; $n = 1+\varphi$ where φ is the Brooks-Corey parameter for the pore-size index; $m = 1-\frac{1}{n}$; ϕ is the soil porosity; and θ_r is the residual soil moisture. For this application, the wilting and vegetation stress pressure was set to -3 and -0.03 MPa, respectively.

Acknowledgments

The authors are grateful for the financial support received from the Australian Research Council (grant LP0991280), the Department of Sustainability and Environment, Victoria, Australia; the Department of Primary Industries, Victoria, Australia; and the Bureau of Meteorology, Australia. The authors thank Murugesu Sivapalan, Stan Schymanski, and an anonymous reviewer for their valuable comments and suggestions. The authors also thank Robert M. Argent of the Bureau of Meteorology, Australia, for his review of the paper prior to submission.

References

Anderies, J. M. (2005), Minimal models and agroecological policy at the regional scale: An application to salinity problems in southeastern Australia, *Reg. Environ. Change*, *5*(1), 1–17, doi:10.1007/s10113-004-0081-z.

Anderies, J. M., M. A. Janssen, and B. H. Walker (2002), Grazing management, resilience, and the dynamics of a fire-driven rangeland system, *Ecosystems*, *5*(1), 23–44.

Anderies, J. M., P. Ryan, and B. H. Walker (2006), Loss of resilience, crisis, and institutional change: Lessons from an intensive agricultural system in southeastern Australia, *Ecosystems*, *9*(6), 865–878, doi:10.1007/s10021-006-0017-1.

Beisner, B. E., D. T. Haydon, and K. Cuddington (2003), Alternative stable states in ecology, *Frontiers Ecol. Environ.*, *1*(7), 376, doi:10.2307/3868190.

Dhooge, A., W. Govaerts, and Y. A. Kuznetsov (2003), MATCONT: A MATLAB package for numerical bifurcation analysis of ODEs, *ACM Trans. Math. Software*, *29*(2), 141–164.

D'Odorico, P., F. Laio, and L. Ridolfi (2005), Noise-induced stability in dryland plant ecosystems, *Proc. Natl. Acad. Sci. U. S. A.*, *102*(31), 10,819–10,822, doi:10.1073/pnas.0502884102.

D'Odorico, P., F. Laio, L. Ridolfi, and M. Lerdau (2008), Biodiversity enhancement induced by environmental noise, *J. Theor. Biol.*, *255*(3), 332–337.

D'Odorico, P., V. Engel, J. Carr, S. Oberbauer, M. Ross, and J. Sah (2011), Tree-grass coexistence in the everglades freshwater system, *Ecosystems*, *14*(2), 298–310, doi:10.1007/s10021-011-9412-3.

Eagleson, P. S. (1978), Climate, soil, and vegetation—1. Introduction to water balance dynamics, *Water Resour. Res.*, *14*(5), 705–712.

Guttal, V., and C. Jayaprakash (2007), Impact of noise on bistable ecological systems, *Ecol. Modell.*, *201*(3–4), 420–428, doi:10.1016/j.ecolmodel.2006.10.005.

Guttal, V., and C. Jayaprakash (2009), Spatial variance and spatial skewness: Leading indicators of regime shifts in spatial ecological systems, *Theor. Ecol.*, *2*(1), 3–12, doi:10.1007/s12080-008-0033-1.

Harbaugh, A. W., E. R. Banta, M. C. Hill, and M. G. McDonald (2000), MODFLOW-2000, the U.S. Geological Survey modular ground-water model—User guide to modularization concepts and the ground-water flow process, *U.S. Geol. Surv. Open File Rep. 2000–92*, 121 pp.

Heffernan, J. (2008), Wetlands as an alternative stable state in desert streams, *Ecology*, *89*(5), 1261–1271, doi:10.1890/07-0915.1.

Holling, C. S. (1973), Resilience and stability of ecological systems, *Annu. Rev. Ecol. Syst.*, *4*, 1–23, doi:10.1146/annurev.es.04.110173.000245.
Jeffrey, S. J., J. O. Carter, K. B. Moodie, and A. R. Beswick (2001), Using spatial interpolation to construct a comprehensive archive of Australian climate data, *Environ. Modell. Software*, *16*(4), 309–330, doi:10.1016/S1364-8152(01)00008-1.
Kandel, D. D., A. W. Western, and R. B. Grayson (2005), Scaling from process timescales to daily time steps: A distribution function approach, *Water Resour. Res.*, *41*, W02003, doi:10.1029/2004WR003380.
Kavetski, D., and G. Kuczera (2007), Model smoothing strategies to remove microscale discontinuities and spurious secondary optima in objective functions in hydrological calibration, *Water Resour. Res.*, *43*, W03411, doi:10.1029/2006WR005195.
Laio, F., A. Porporato, L. Ridoland, and I. Rodriguez-Iturbe (2001), Plants in water-controlled ecosystems: Active role in hydrologic processes and response to water stress II. Probabilistic soil moisture dynamics, *Adv. Water Resour.*, *24*, 707–723, doi:10.1016/S0309-1708(01)00005-7.
May, R. M. (1977), Thresholds and breakpoints in ecosystems with a multiplicity of stable states, *Nature*, *269*(5628), 471–477.
Peterson, T. J. (2009), Multiple hydrological steady states and resilience, PhD thesis, Dep. of Civil and Environ. Eng., Univ. of Melbourne, Parkville, Australia. [Available at http://repository.unimelb.edu.au/10187/8540.]
Peterson, T. J., R. M. Argent, A. W. Western, and F. H. S. Chiew (2009), Multiple stable states in hydrological models: An ecohydrological investigation, *Water Resour. Res.*, *40*, W03406, doi:10.1029/2008WR006886.
Peterson, T. J., A. W. Western, and R. M. Argent (2012), Analytical methods for ecosystem resilience: A hydrological investigation, *Water Resour. Res.*, *48*, W10531, doi:10.1029/2012WR012150.
Press, W. H., S. A. Teukolsky, W. T. Vetterling, and B. P. Flannery (2007), *Numerical Recipes: The Art of Scientific Computing*, 3rd ed., Cambridge Univ. Press, New York.
Rennermalm, A. K., J. M. Nordbotten, and E. F. Wood (2010), Hydrologic variability and its influence on long-term peat dynamics, *Water Resour. Res.*, *46*, W12546, doi:10.1029/2009WR008242.
Ridders, C. J. F. (1982), Accurate computation of F′(x) and F′(x) F″(x), *Adv. Eng. Software*, *4*(2), 75–76.
Ridolfi, L., P. D'Odorico, and F. Laio (2006), Effect of vegetation-water table feedbacks on the stability and resilience of plant ecosystems, *Water Resour. Res.*, *42*, W01201, doi:10.1029/2005WR004444.
Runyan, C. W., and P. D'Odorico (2010), Ecohydrological feedbacks between salt accumulation and vegetation dynamics: Role of vegetation-groundwater interactions, *Water Resour. Res.*, *46*, W11561, doi:10.1029/2010WR009464.
Runyan, C. W., and P. D'Odorico (2012), Ecohydrological feedbacks between permafrost and vegetation dynamics, *Adv. Water Resour.*, *49*, 1–12, doi:10.1016/j.advwatres.2012.07.016.
Runyan, C. W., and P. D'Odorico (2013), Positive feedbacks and bistability associated with phosphorus-vegetation-microbial interactions, *Adv. Water Resour.*, *52*, 151–164, doi:10.1016/j.advwatres.2012.09.004.
Scheffer, M., and S. R. Carpenter (2003), Catastrophic regime shifts in ecosystems: Linking theory to observation, *Trends Ecol. Evol.*, *18*(12), 648–656.
Shampine, L., and M. Reichelt (1997), The MATLAB ODE suite, *SIAM J. Sci. Stat. Comput.*, *18*(1), 1–22.
Troch, P. A., C. Paniconi, and E. E. van Loon (2003), Hillslope-storage Boussinesq model for subsurface flow and variable source areas along complex hillslopes: 1. Formulation and characteristic response, *Water Resour. Res.*, *39*(11), 1316, doi:10.1029/2002WR001728.
van Genuchten, M. T. (1980), A closed-form equation for predicting the hydraulic conductivity of unsaturated soils, *Soil Sci. Soc. Am. J.*, *44*(5), 892–898.
van Nes, E. H., and M. Scheffer (2005), Implications of spatial heterogeneity for catastrophic regime shifts in ecosystems, *Ecology*, *86*(7), 1797–1807.
Walker, B. H., C. S. Holling, S. R. Carpenter, and A. Kinzig (2004), Resilience, adaptability and transformability in social-ecological systems, *Ecol. Soc.*, *9*(2), 5. [Available at: http://www.ecologyandsociety.org/vol9/iss2/art5/.].